the
electronic
journal of
chemistry

The Crystal Structure of the New Layered Alloy $(CuGa)_{0.52}TaSe_2$ Studied by SEM, DTA, and XRPD

Gerzon E. Delgado* [ID] [a], Sonia Durán [ID] [b], Jennifer A. Aitken [ID] [c], Marcos Muñoz [ID] [b], and Pedro Grima-Gallardo [ID] [d,e,f]

The new $(CuGa)_{0.52}TaSe_2$ alloy was synthesized by the melt and annealing technique and studied by SEM, DTA, and XRPD techniques. Its structure has been refined by the Rietveld method using X-ray powder diffraction data. This compound crystallizes in the hexagonal space group P-6m2 (N° 187) with unit cell parameters a = 3.648(2) Å, c = 13.568(4) Å, V = 156.4(1) Å^3, Z = 2. The crystal structure is based on the MoS_2-type of stacking of $TaSe_2$ layers with a partial ordering of Cu and Ga cations over the tetrahedral sites. The powder pattern was composed of 63.9% of the principal phase $(CuGa)_{0.52}TaSe_2$ and 26.3% of $CuGaSe_2$, 9.8% of $TaSe_3$, as the secondary phases.

Graphical abstract
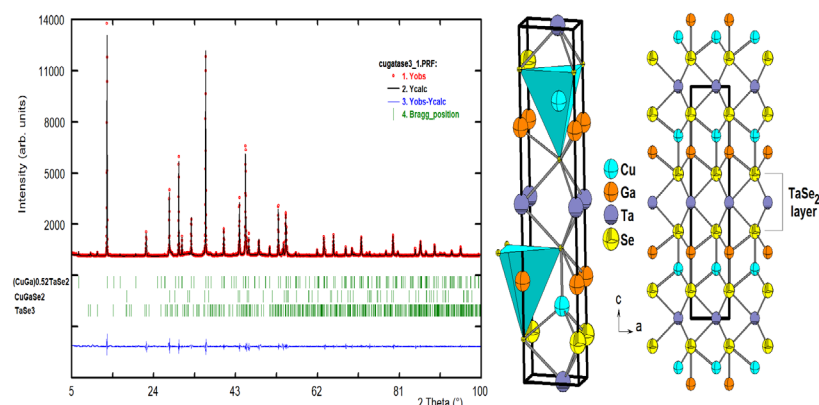
Keywords

$Mo-S_2$ type
Alloys
Crystal structure
X-ray powder diffraction

1. Introduction

The successful manufacture of a 2D single-layer graphene [1] has led to an interest in the study of two-dimensional monolayer materials. In particular, the transition metal chalcogenides and their intercalated compounds have attracted interest due to their low-dimensional electronic properties leading to the development of superconductivity, electrical resistivity, thermal expansion, and optical properties [2-4]. Transition metal dichalcogenides are layered materials that are composed of transition metals (TR) and chalcogens of the group VIA (O, S, Se, Te), which have been found to crystallize in different polytypes [5]. Among them, MoS_2 has attracted considerable attention due to its important role in the lithium-ion battery, among other applications [6].

On the other hand, $CuGaSe_2$, an I-III-VI$_2$ semiconductor material with a tetragonal structure [7], has been widely studied because of its applications in the photovoltaic industry [8-9]. When a ternary chalcogenide semiconductor (I-III-VI$_2$) is diversified with a binary transition metal (TR-VI) is possible to obtain alloys of the type $(I-III-VI_2)_{1-x}(II-VI)_x$ [10],

[a] Laboratorio de Cristalografía, Departamento de Química, Facultad de Ciencias, Universidad de Los Andes, Mérida 5101, Venezuela. [b] Universidad Centro-Occidental "Lisandro Alvarado", Barquisimeto 3001, Venezuela. [c] Department of Chemistry and Biochemistry, Duquesne University, Pittsburgh 15282, USA. [d] Centro de Estudios en Semiconductores, Departamento de Física, Facultad de Ciencias, Universidad de Los Andes, Mérida 5101, Venezuela. [e] Centro Nacional de Tecnologías Ópticas (CNTO), Mérida 5101, Venezuela. [f] Centro de Investigaciones de Astronomía (CIDA), Mérida 5101, Venezuela. Corresponding author. E-mail: **gerzon@ula.ve**

which present interesting crystal structures and diverse physical properties [11-22]. These types of semiconductors combined with magnetic behavior give place to the so-called "diluted magnetic semiconductors" or "semi-magnetic semiconductors", which have been largely investigated in the last years due to their possible application in spintronic devices [23]. Besides, chalcogen-based (VI = S, Se, Te) begin to be studied as potential trainers of "wide bandgap semiconductors", which are essential for electronic devices and energy applications because of their high optical transparency, controllable carrier concentration, and tunable electrical conductivity [24]. On the other hand, Ta-based chalcogenides, are usually used to form alloys with applicable properties due to their high melting point [5, 25].

In this work, and as part of ongoing structural studies on semiconductors of the system $(Cu-III-VI_2)_{1-x}(Ta-VI)_x$ [14-18], we report the synthesis and structural analysis of the quaternary semiconductor with a composition $(CuGa)_{0.52}TaSe_2$. This compound is a new member of the $(CuGaSe_2)_{1-x}(TaSe)_x$ family, which is a related phase of the hexagonal compound $2H-Cu_{0.52}TaSe_2$ [5], with a similar structure to the MoS_2 layered phase.

2. Results and Discussion

Table 1 shows summarized the average atomic percentages of the SEM analysis performed on three different regions of the ingot synthetized. In this case, upper, medium, and low parts of the ingot were analyzed to assure the homogeneity of the measurement. Besides, for each region, five different measurements were made, and the average had been taken over a total of fifty measurements. The mean experimental stoichiometry observed has been calculated as $(CuGa)_{0.52}TaSe_2$. Fig. 1 shows the microphotography of this phase where can be observed the platelets that confirm the laminar character of the crystal structure for this phase and clearly it shows a hexagonal shape.

Table 1. SEM experimental results for $(CuGaSe_2)_{1-x}(TaSe)_x$ alloy system for x = ½.

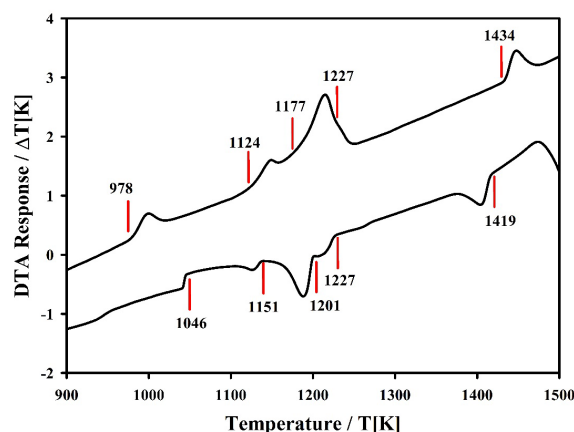| Nominal stoichiometry (%)	Experimental stoichiometry (%)
Cu=07.39	Cu = 08.8 ± 0.5
Ga=07.39	Al = 09.4 ± 0.6
Ta=28.41	Ta = 26.5 ± 1.4
Se=56.82	Se = 55.3 ± 0.6
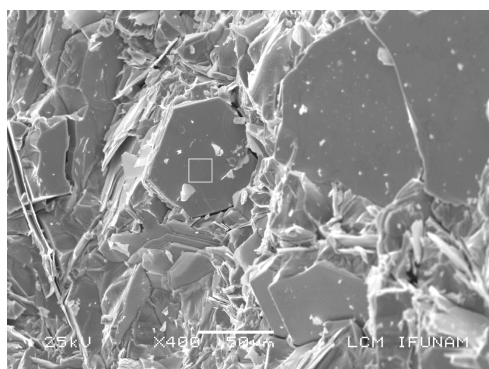
Fig. 1. Microphotography of the $(CuGa)_{0.52}TaSe_2$ alloy.

Fig. 2 shows the DTA heating and cooling cycles plots for $(CuGaSe_2)_{1-x}(TaSe)_x$ alloy with x= ½. The differential thermal

analysis (DTA) indicates that this compound melts at 1434 K.

Fig. 2. DTA heating (top) and cooling (bottom) cycles for $(CuGaSe_2)_{1-x}(TaSe)_x$ alloy with x = ½.

X-ray powder pattern is shown in Fig. 3. A search in the PDF-ICDD database [26] indicates that the powder pattern also contains small amounts of $CuGaSe_2$ (PDF 01-076-1735) and $TaSe_3$ (PDF 00-18-1310). The Bragg intense peaks corresponding to the phase of interest were indexed in a hexagonal cell with *a*= 3.640 Å and *c*= 13.562 Å, using the program Dicvol04 [27]. A revision of the diffraction lines of the main phase taking into account the sample composition and unit cell parameters suggested that this material is isostructural with the phase $2H-Cu_{0.52}TaSe_2$, which crystallizes in the space group *P-6m2* (Nº 187) [5].
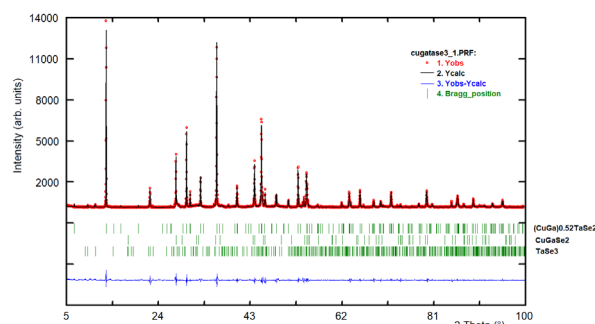
Fig. 3. Rietveld refinement plot of the new phase $(CuGa)_{0.52}TaSe_2$ together with the secondary phases $CuGaSe_2$ and $TaSe_3$. The lower trace is the difference curve between observed and calculated patterns. The Bragg reflections are indicated by vertical bars.

Rietveld refinement was performed [28] using the program Fullprof Suite [29] by applying a Cox-Hastings pseudo-Voigt function [30]. The background was fitted using a linear interpolation between a set of background points. The angular dependence of the peak full width at half maximum (FWHM) was described by Caglioti's formula [31]. The thermal motion of the atoms was described by one overall isotropic temperature factor for each phase. The atomic coordinates of $Cu_{0.52}TaSe_2$ [5] were used as a starting model for the quaternary $(CuGa)_{0.52}TaSe_2$ where the Cu and Ga atoms occupy the Wickoff sites *2i* and *2g*, respectively. The atomic positions of the ternary $CuGaSe_2$ [32] and the binary $TaSe_3$ [33] were included as secondary phases in the refinement. The results of the Rietveld refinement are summarized in Table 2. Rietveld refinement converged to the following weight fraction

percentages: $(CuGa)_{0.52}TaSe_2$ (63.9%), $CuGaSe_2$ (26.3%), and $TaSe_3$ (9.8%). It should be noted that the occupancy factors for Cu and Ga cations are in good agreement with the values found in chemical analysis (see Table 3) and the stoichiometry of this alloy is confirmed: $(CuGa)_{0.52}TaSe_2$. Fig. 3 shows the observed, calculated, and difference profile for the final cycle of Rietveld refinement. Atomic coordinates and isotropic temperature factor for the new phase $(CuGa)_{0.52}TaSe_2$ are shown in Table 3.

The crystal structure is based on the MoS_2 type of stacking of $TaSe_2$ layers with a partial ordering of Cu and Ga cations over the tetrahedral sites. Fig.4a shown the tetrahedral around the Cu and Ga cations and Fig. 4b shown the $TaSe_2$ layer at the center. $(CuGa)_{0.52}TaSe_2$ is a new chalcogenide compound, related to the layered $2H-Cu_{0.52}TaSe_2$ phase, with potential use as a wide bandgap semiconductor [24].

Molecular formula	$(CuGa)_{0.52}TaSe_2$
Molecular weight (g/mol)	373.52
System	hexagonal
Space group	*P-6m2* (187)
D_{calc} (g/cm^{-3})	7.93
a (Å)	3.648(2)
c (Å)	13.568(4)
V (Å^3)	156.4(1)
Z	2
R_{exp} (%)	7.2
R_p (%)	8.0
R_{wp} (%)	8.8
S	1.2
R_B (%)	8.1

$R_{exp} = 100[(N+C)/\sum_w(y_{obs}^2)]^{1/2}$ $R_p = 100 \sum|y_{obs}-y_{calc}|/\sum|y_{obs}|$ S = $[R_{wp}/R_{exp}]$. $R_{wp} = 100 [\sum_w|y_{obs}-y_{calc}|^2/\sum_w|y_{obs}|^2]^{1/2}$ $R_B = 100 \sum_k|I_k-Ic_k|/\sum_k|I_k|$ N-P+C= degrees of freedom

Table 2. Rietveld refinement results for $(CuGa)_{0.52}TaSe_2$.

Table 3. Atomic coordinates (Å) and isotropic temperature factors for $(CuGa)_{0.52}TaSe_2$, derived from the Rietveld refinement.

Atom	Ox.	Site	x	y	z	foc	B (Å^2)
Cu	+1	2i	⅔	⅓	0.2125(6)	0.26(2)	0.5(4)
Ga	+1	2g	0	0	0.2844(6)	0.26(2)	0.5(4)
Ta1	+2	1b	0	0	½	1	0.5(4)
Ta2	+2	1e	⅔	⅓	0	1	0.5(4)
Se1	-2	2i	⅔	⅓	0.3760(6)	1	0.5(4)
Se2	-2	2g	0	0	0.1206(6)	1	0.5(4)
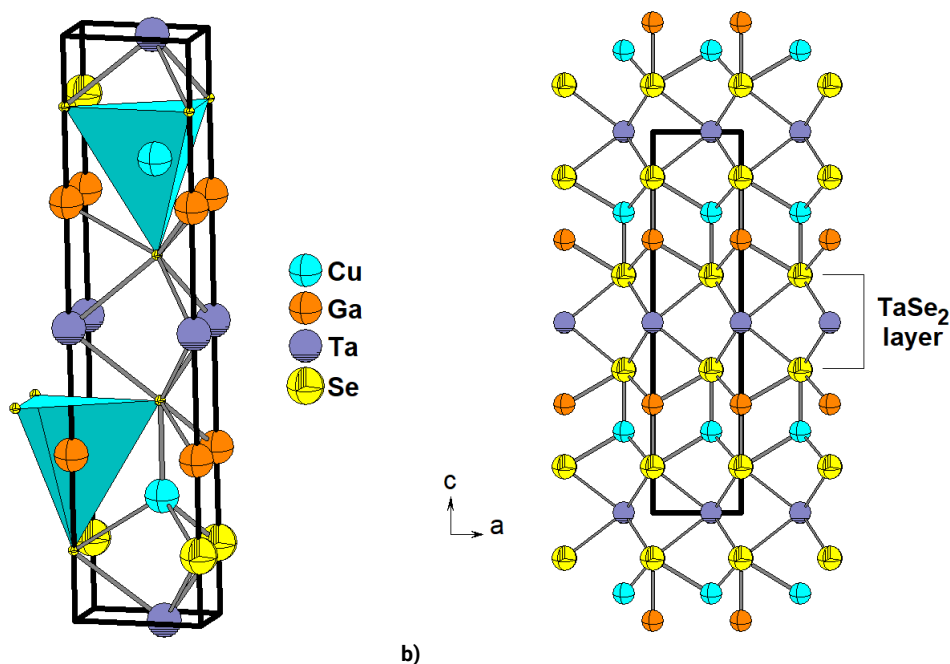
Fig. 4. a) Unit cell representation for $(CuGa)_{0.52}TaSe_2$, showing the tetrahedral around the Cu and Ga cations, and b) Packing showing the $TaSe_2$ layer.

3. Material and Methods

3.1. Synthesis

Starting materials (Cu, Ga Ta, and Se) with nominal purity of 99.99 wt. % (GoodFellow) in the stoichiometric ratio were mixed in an evacuated (10^{-4} Torr) and sealed quartz tube with the inner walls previously carbonized to prevent the chemical reaction of the elements with quartz. The quartz ampoule is heated until 493 K (melting point of Se) keeping this temperature for 48 h and shaking all the time using an electromechanical motor. This procedure guarantees the formation of binary species at low temperatures avoiding the

existence of Se free gas at high temperatures, which could produce explosions or Se deficiency in the ingot. Then the temperature was slowly increased until 1423 K, with the mechanical shaker always connected for better mixing of the components. After 24 h, the cooling cycle begins until the anneal temperature (800K) with the mechanical shaker is disconnected. The ampoule is keeping at the annealing temperature for 1 month to assure thermal equilibrium. Then the furnace is switching off.

3.2. Scanning Electron Microscopy

Stoichiometric relations of the sample were investigated by scanning electron microscopy (SEM) technique, using a Hitachi S2500 equipment. The microchemical composition was found by an energy-dispersive x-ray spectrometer (EDS) coupled with a computer-based multichannel analyzer (MCA, Delta III analysis, and Quantex software, Kevex). For the EDS analysis, $K\alpha$ lines were used. The accelerating voltage was 15 kV. The samples were tilted 35 degrees. A standardless EDS analysis was made with a relative error of $\pm$ 5-10% and detection limits of the order of 0.3 wt %, where the k-ratios are based on theoretical standards.

3.3. Differential Thermal Analysis

Differential Thermal Analysis (DTA) measurements were carried out in a fully automatic Perkin-Elmer apparatus, which consists of a Khantal resistance furnace (T_{max}=1650 K) equipped with Pt/Pt-Rh thermocouples and an informatics system for the automatic acquisition data. The internal standard used was a high purity (99.99 wt. %) piece of gold. The temperature runs have been performed from ambient temperature to 1400−1500 K, which is the recommended operative limit. The heating rate was controlled electronically to 20 Kh^{-1}; the cooling rate was given by the natural cooling of the furnace after switching off. From the thermogram, transition temperatures were manually obtained from the ΔT vs. T graph with the criteria that the transition occurs at the intersection of the baseline with the slope of the thermal transition peak, as usual. The maximum error committed in the determination of transition temperatures by this method was estimated to be $\pm$ 10 K.

3.4. X-Ray Powder Diffraction

X-ray powder diffraction data were collected using a diffractometer Siemens D5005 equipped with a graphite monochromator (CuKα, λ= 1.54059 Å) at 40 kV and 20 mA. Quartz was used as an external standard. The sample was scanned from 5-100° 2θ, with a step size of 0.02° and counting time of 20 s. The peak positions were extracted utilizing single-peak profile fitting carried out through the Bruker analytical software. For the Rietveld refinement, the whole diffraction data was used.

4. Conclusions

The system $(CuGaSe_2)_{1-x}(TaSe)_x$ with x = ½ has been synthesized and studied by SEM, DTA, and XRPD techniques. A new alloy with experimental stoichiometry $(CuGa)_{0.52}TaSe_2$ were identified and refined. This alloy crystallizes in the hexagonal structure, space group *P-6m2* (N° 187), with unit cell parameters a = 3.468(2) Å, c = 13.568(4) Å, V = 156.4(1) Å^3. The powder pattern was composed of 63.9% of $(CuGa)_{0.52}TaSe_2$, with $CuGaSe_2$ 10.8% and $TaSe_3$ 26.3% as secondary phases.

Author Contributions

Gerzon E. Delgado: Conceptualization, Writing-Review & Editing, Supervision. Sonia Durán: Methodology. Jennifer A. Aitken: Methodology. Marcos Muñoz: Writing-Review & Editing. Pedro Grima-Gallardo: Writing-Review & Editing.

References and Notes

[1] Novoselov, K. S.; Geim, A. K.; Morozov, S. V.; Jiang, D.; Zhang, Y.; Dubonos, S. V.; Grigorieva, I. V.; Filrsov, A. A. *Science* **2004**, *306*, 666. **[Crossref]**

[2] Monceau, P. *Adv. Phys*. **2012**, *61*, 325. **[Crossref]**

[3] Tomić, S.; Dressel, M. *Rep. Prog. Phys*. **2015**, *78*, 096501. **[Crossref]**

[4] Han, G. H.; Duong, D. L.; Keum, D. H.; Yun, S. J.; Lee, Y. H. *Chem. Rev*. **2018**, *118*, 6297. **[Crossref]**

[5] Ali, S. I.; Mondal, S.; van Smaalen, S. *Z. Anorg. Allg. Chem*. **2015**, *641*, 464. **[Crossref]**

[6] Kan, M.; Wang, J. Y.; Li, X. W.; Zhang, S. H.; Li, Y. W.; Kawazoe, Y.; Sun, Q.; Jena, P. *J. Phys. Chem. C* **2014**, *118*, 1515. **[Crossref]**

[7] Mandel, L.; Tomlinson, R. D.; Hampshire, M. J. *J. Appl. Cryst*. **1977**, *10*, 130. **[Crossref]**

[8] Chopra, K. L.; Paulson, P. D.; Dutta, V. *Prog. Photovoltaics Res. Appl*. **2004**, *12*, 69. **[Crossref]**

[9] Nayak, P. K.; Bisquert, J; Cahen, D. *Avd. Mat*. **2011**, *23*, 2870. **[Crossref]**

[10] Parthé E. Wurtzite and sphalerite structures. In: Intermetallic Compounds, Principles and Applications, v. 1. Westbrook, J. H.; Fleischer, R. L., eds. Chichester, UK: John Wiley & Sons, 1995

[11] Grima-Gallardo, P.; Molina, L.; Quintero, M.; Tovar, R.; Ruiz, J.; Quintero, E.; Delgado, G. E.; Maury, L. *Phys. Stat. Sol. B* **2000**, *220*, 377. **[Crossref]**

[12] Grima-Gallardo, P.; Cárdenas, K.; Quintero, M.; Ruiz, J.; Delgado, G. E. *Mater. Res. Bull*. **2001**, *36*, 861. **[Crossref]**

[13] Grima-Gallardo, P.; Muñoz, M.; Delgado, G. E.; Briceño, J. M.; Ruiz, J. *Phys. Stat. Sol. B* **2001**, *241*, 1789. **[Crossref]**

[14] Grima-Gallardo, P.; Muñoz, M.; Durán, S.; Delgado, G. E.; Quintero, M.; Ruiz, J. *Mater. Res. Bull*. **2007**, *42*, 2067. **[Crossref]**

[15] Grima-Gallardo, P.; Muñoz, M.; Durán, S.; Delgado, G. E.; Quintero, M.; Briceño, J. M.; Ruiz, J. *Phys. Stat. Sol. A* **2007**, *204*, 1093. **[Crossref]**

[16] Mora, A. J.; Delgado, G. E.; Grima-Gallardo, P. *Phys. Stat. Sol. A* **2007**, *204*, 547. **[Crossref]**

[17] Delgado, G. E.; Mora, A. J.; Grima-Gallardo, P.; Quintero, M. *J. Alloys Comp*. **2008**, *454*, 306. **[Crossref]**

[18] Delgado, G. E.; Mora, A. J.; Contreras, J. E.; Grima-Gallardo, P.; Durán, S.; Muñoz, M.; Quintero, M. *Cryst. Res. Technol*. **2009**, *44*, 548. **[Crossref]**

[19] Delgado, G. E.; Mora, A. J.; Grima-Gallardo, P.; Durán, S.; Muñoz, M.; Quintero, M. *Bull. Mater. Sci*. **2010**, *33*, 637. **[Crossref]**

[20] Delgado, G. E.; Quintero, E.; Tovar, R.; Grima-Gallardo, P.; Quintero, M. *J. Alloys Comp*. **2014**, *613*, 143. **[Crossref]**

[21] Delgado, G. E.; Mora, A. J.; Grima-Gallardo, P.; Muñoz, M.; Durán, S.; Quintero, M.; Briceño, J. M. *Bull. Mater. Sci*. **2015**, *38*, 1061. **[Crossref]**

[22] Grima-Gallardo, P.; Torres, S.; Quintero, M.; Nieves, L.; Moreno, E.; Delgado, G. E. *J. Alloys Comp*. **2015**, *630*, 146. **[Crossref]**

[22] Grima-Gallardo, P.; Muñoz, M.; Durán, S.; Delgado, G. E.; Pérez-Cappé, E.; Aitken, J. A. *Senhri J. Mult. Stud*. **2020**, *5*, 1. **[Crossref]**

[23] Pearton, S. J.; Abernathy, C. R.; Norton, D. P.; Hebard, A. F.; Park, Y. D.; Boatner, L. A.; Budai, J. D. *Mater. Sci. Eng*. **2003**, *R40*, 137. **[Crossref]**

[24] Woods-Robinson, R.; Yanbing Han, Y.; Zhang, H.; Ablekim, T.; Khan, K.; Persson, K.; Zakutayev, A. *Chem. Rev*. **2020**, *120*, 4007. **[Crossref]**

[25] Hayashi, K.; Tanico, Y.; Kawachi, K.; Nakata, Y.; Inoue, K.; Maeda, N. *J. Alloys Compd*. **2007**, *442*, 117. **[Crossref]**

[26] International Centre for Diffraction Data (ICDD), Powder Diffraction File (Set 1-65). Newtown Square, PA, USA, **2013**.

[27] Boultif, A.; Louer, D. *J. Appl. Cryst*. **2004**, *37*, 724. **[Crossref]**

[28] Rietveld, H. M. *J. App. Cryst*. **1969**, *2*, 65. **[Crossref]**

[29] Rodriguez-Carvajal, *J. Phys. B: Cond. Matter* **1993** *192*, 55. **[Crossref]**

[30] Thompson, P.; Cox, D. E.; Hastings, J. B. *J. App. Cryst*. **1987**, *20*, 79. **[Crossref]**

[31] Cagliotti, G.; Paoletti, A.; Ricci, F. P. *Nucl. Instrum*. **1958**, *3*, 223. **[Crossref]**

[32] Mandel, L.; Tomlinson, R. D.; Hampshire, M. J. *J. Appl. Cryst*. **1977**, *10*, 130. **[Crossref]**

[33] Bjerkelund, E.; Kjekshus, A. *Acta Chem. Scand*. **1965**, *19*, 701. **[Crossref]**

How to cite this article